ACS APPLIED MATERIALS & INTERFACES

Research Article

Cite This: ACS Appl. Mater. Interfaces 2018, 10, 32239−32246

www.acsami.org

# Preparation of Spherical Mordenite Zeolite Assemblies with Excellent Catalytic Performance for Dimethyl Ether Carbonylation

Lingyun Li,[†,‡] Quanyi Wang,[†] Hongchao Liu,[†] Tantan Sun,[†,‡] Dong Fan,[†] Miao Yang,[†] Peng Tian,*[,†] and Zhongmin Liu*[,†]

[†]National Engineering Laboratory for Methanol to Olefins, Dalian National Laboratory for Clean Energy, Dalian Institute of Chemical Physics, Chinese Academy of Sciences, Dalian 116023, People's Republic of China

[‡]University of Chinese Academy of Sciences, Beijing 100049, People's Republic of China

Supporting Information

**ABSTRACT:** Millimeter-sized spherical mordenite (MOR) zeolite with good mechanical strength was successfully prepared via vapor-assisted transformation of Na- and Al-doped $SiO_2$ spheres. It is demonstrated that the precursor prepared by vacuum impregnation is essential for the achievement of well-retained morphology; the presence of organic amine (such as TEAOH, TMAOH, and HMI) in the vapor can help promote the crystallization, avoid the core−shell morphology, and improve the zeolite Si/Al ratio, although the MOR crystal morphology in the spherical products varies with the choice of organic amines. The resultant MOR-TEAOH spheres, which were synthesized under the assistance of TEAOH, possess large amount of Brønsted acid sites in the 8-MR side pockets (0.76 mmol/g), which is about 3 times higher than in the 12-MR main channels. The preferential siting of $H^+$ sites in the 8-MR helps MOR-TEAOH show excellent catalytic performance in the DME carbonylation reaction. A 90% of DME steady conversion is observed on MOR-TEAOH, which is obviously higher than that on commercial sample (23%). This work offers millimeter-scale spherical MOR with good mechanical strength and excellent catalytic performance, which is very promising for the industrial applications.

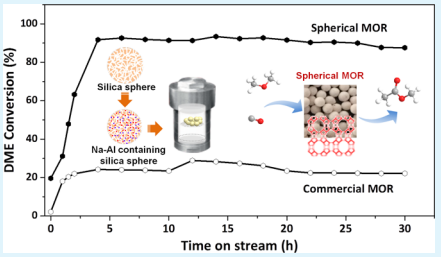


**KEYWORDS:** *mordenite, spherical zeolite, synthesis, acid distribution, DME carbonylation*

## 1. INTRODUCTION

Zeolites are microporous crystalline aluminosilicates with uniform pores, intrinsic acidity, and shape selectivity, which have been widely employed as heterogeneous catalysts in the chemical industries. Mordenite (MOR) zeolite, consisting of a straight 12-membered ring (MR) channels with intersecting 8-MR channels (side pockets), is one of the most important zeolites that finds industrial applications in catalytic processes of toluene disproportionation, hydroisomerization, etc. Recently, MOR zeolite further attracts considerable attention due to its prominent catalytic performance in the dimethyl ether (DME) carbonylation to methyl acetate (MAc), and the Brønsted acid sites located in the 8-MR side pockets were revealed to be the unique active sites for the reaction.[1−4] DME carbonylation reaction together with the subsequent hydrogenation of MAc to ethanol opens a new ethanol production route from nongrain feedstocks such as coal and natural gas.[5,6]

In the attempt to improve the catalytic performance of MOR zeolites in the DME carbonylation reaction, efforts were made to synthesize nanosized/hierarchical MOR to enhance the mass transfer.[7−10] However, because of the preferential growth of the crystals along the 12-MR channels (*c*-axis direction), the resultant materials generally show nanoslab/nanorod morphology with inhibited growth mainly in the *a*-axis and *b*-axis directions rather than in the *c*-axis direction. This thus gives a limited enhancement on the mass transfer. On the other hand, given that the siting and distribution of framework Al atoms in the zeolites control the location of the Brønsted acid sites,[11] it would be an effective way to improve the catalytic performance of MOR zeolites by tuning the Al siting. Hitherto, it is recognized that the siting of Al atoms in the framework is not random and depends on the zeolite synthesis conditions. But, the related research is mainly focused on few zeolites such as ZSM-5[12,13] and ZSM-35[14−16] and less for MOR zeolite. It would be valuable to find an effective way to tune the Al siting in the framework of MOR zeolite and maximize its distribution in the 8-MR side pockets.

For the practical applications of zeolite catalysts, a shaping process is generally indispensable, in which the zeolite powders are processed into appropriate size and shape with enough mechanical strength to satisfy the requirements of industrial reactors. Inorganic binders such as alumina, silica, or clay are commonly introduced to help the molding process and improve the strength of the shaped catalysts. However, introduction of inorganic binders will inevitably dilute the zeolite content in the catalysts and sometimes even causes

Received: July 16, 2018
Accepted: August 29, 2018
Published: August 29, 2018






DOI: 10.1021/acsami.8b11823
ACS Appl. Mater. Interfaces 2018, 10, 32239−32246

partial blocking of zeolite micropores.[17,18] To overcome these problems, attempts have been made to prepare shaped zeolite catalysts without binders, the strategies of which include pressure forming,[19] gel-casting,[20] and self-assembling of zeolite nanocrystals with organic polymer as the scaffold. These approaches, however, require relatively complex preparation procedures and often generate products with limited mechanical strength. Another strategy is *in situ* crystallization of the preshaped/pretreated precursors.[21−23] Previous studies on the crystallization of precursors into zeolites with well-retained morphology were mainly limited to ZSM-5 with higher Si/Al ratios.[23] Reports on the intact transformation of preshaped precursors to zeolites with medium/low Si/Al ratios are lacking. This is possibly due to the higher synthetic alkalinity for medium/low Si/Al ratio zeolites, hindering the morphology preservation of the silica precursors. This phenomenon is more pronounced when the precursors are in millimeter scale because a homogeneous crystallization from the shell to the core is difficult to achieve.

Herein, we report a facile approach to prepare MOR spheres via vapor-assisted method by using commercial millimeter-sized $SiO_2$ spheres (2−3 mm) as the precursor. Such millimeter-scale spheres are desirable for industrial fixed bed reactors because they could be smoothly loaded into the reactors and help avoid channel flow. Moreover, the obtained spherical MOR product shows a preferential locating of Brønsted acid sites in the 8-MR side pockets, which is beneficial for its catalytic application in the DME carbonylation reaction.

## 2. EXPERIMENTAL SECTION

**Chemicals and Reagents.** Porous silica spheres ($SiO_2$, 98.5 wt %) were purchased from Qingdao Shiji Haiyang Desiccant Co., Ltd.. Sodium aluminate ($NaAlO_2$, 45 wt %), tetraethylammonium hydroxide (TEAOH, 35 wt %), and tetramethylammonium hydroxide (TMAOH, 25 wt %) were purchased from Tianjin Damao Chemical Reagent Factory. Hexamethylenimine (HMI, 99 wt %) and triethylamine (TEA, 99 wt %) were purchased from Tianjin Damao Chemical Reagent Factory. Sodium hydroxide (NaOH, 96 wt %) was purchased from Sinopharm Chemical Reagent Co., Ltd. All the chemicals were used as received without further purification.

**Synthesis of Spherical MOR Zeolites (Denoted as MOR-TEAOH).** Sodium aluminate was first added into deionized water and stirred until the solution was clear. Then, NaOH was added to the solution and stirred for 10 min, obtaining a clear solution with a molar composition of $Al_2O_3/Na_2O/H_2O$ = 1/1.6/38. Ten grams of silica spheres were impregnated into the solution for 10 min under vacuum. The spheres were then separated and dried at room temperature to obtain spherical precursor with molar composition of 20.5−21.0 $SiO_2$:1.0 $Al_2O_3$:1.8 $Na_2O$. The precursor was then transformed into a Teflon-lined stainless steel autoclave with 4.2 g of TEAOH (containing 2.73 g $H_2O$) and 0.5 g water at the bottom. It is noted that there was no direct contact between the solid phase and the liquid. The autoclave was heated at 175 °C for 72 h under static condition. After crystallization, the autoclave was cooled immediately. The solid product was collected, washed with deionized water, and dried at 100 °C overnight. To remove the organic amines, the sample was calcined at 550 °C for 8 h. The H-type sample was obtained by ion exchange with 1 mol/L $NH_4NO_3$ solution repeated 3 times and followed by calcination at 550 °C for 4 h.

**Synthesis of MOR-TMAOH and MOR-HMI.** The synthetic procedures were similar to those of MOR-TEAOH except changing the amines in the liquid at the autoclave bottom. The liquid amounts were 3.65 g of TMAOH (containing 2.73 g $H_2O$) for MOR-TMAOH and 0.99 g of HMI with 1 g of $H_2O$ for MOR-HMI. The crystallization conditions for MOR-TMAOH and MOR-HMI were 170 °C for 84 h.

**Synthesis of MOR-$H_2O$.** The synthetic procedure of MOR-$H_2O$ was similar to that of MOR-TEAOH except using pure water (1 g) as the liquid phase at the autoclave bottom. The precursor was crystallized under 175 °C for 72 h.

**Characterization.** The powder X-ray diffraction (XRD) patterns were carried on a PANalytical X' Pert PRO X-ray diffractometer with Cu K$\alpha$ radiation ($\lambda$ = 0.154059 nm) at 40 kV and 40 mA from 5° to 50°. The morphology of samples were observed on a Hitachi TM3000 and Hitachi SU8020 scanning electron microscope (SEM). The chemical composition was determined by Philips Magix-601 X-ray fluorescence (XRF) spectrometer. Thermogravimetric analysis (TGA) was performed on a TA Q-600 analyzer with a heating rate of 10 °C/min under the air flow. $N_2$ adsorption and desorption measurements were tested on a Micromeritics ASAP 2020 analyzer at −196 °C. The total surface area was calculated by the BET method. The micropore volume and area were calculated by t-plot method. The pore size distribution was evaluated from the adsorption branch of the isotherm by the DFT method. The solid-state nuclear magnetic resonance (NMR) were measured on a Bruker Avance III 600 spectrometer with a 14.1 T wide-bore magnet using a 4 mm WVT double resonances MAS probe with the spinning rate of 12 kHz for $^{27}$Al MAS NMR and 8 kHz for $^{29}$Si MAS NMR. The resonance frequencies of $^{29}$Si and $^{27}$Al are 119.2 and 156.4 MHz. To determine the Brøsnted acid sites in 12-MR (0.7 × 0.65 nm) and in 8-MR side pockets (0.34 × 0.48 nm), $^1$H MAS NMR experiments were carried out, and the corresponding spectra were recorded on the same instrument with a 4 mm H-X double resonances MAS probe. First, all of the samples were dehydrated typically at 420 °C and a pressure below $10^{-3}$ Pa for 12 h. To determine the total amount of Brøsnted acid sites, the samples were cooled to ambient temperature for measurement. When to determine the amount of Brøsnted acid sites in 8-MR, a certain amount of pyridine (kinetic diameter is 0.58 nm) was condensed and frozen inside the samples with liquid nitrogen after the dehydration process. The sample was equilibrated for 0.5 h at ambient temperature and degassed at 50 °C for 1 h to remove the physisorbed probe molecules. $^1$H MAS NMR spectra were recorded using a single pulse sequence with a $\pi/4$ pulse of 2 $\mu$s and a 10 s recycle delay with adamantane (1.74 ppm) as the chemical shift reference. Thirty-two scans were accumulated to obtain a good signal-to-noise ratio. For Brønsted acid density quantification, all samples were weighed, and their $^1$H MAS NMR spectra were resolved by Dmfit software with Gaussian−Lorentz line shapes, also using adamantane as the quantitative external standard, measured under the same NMR acquisition condition. The temperature-programmed desorption of ammonia ($NH_3$-TPD) was tested on Micromeritics Autochem II 2920. The H-type samples (100 mg) were outgassed in a He flow at 650 °C for 60 min and then cooled to 100 °C. The samples were saturated with $NH_3$ at a flow of $NH_3$/He for 60 min, and then the physical adsorbed $NH_3$ was removed by a He flow. The desorption process was operated from 100 to 650 °C with the heating rate of 10 °C/min under the He flow rate of 20 mL/min. The compressive strength of the samples was tested by Dalian Intelligent Testing Instrument Co. Ltd.

**Catalytic Tests.** DME carbonylation experiments were performed in a continuous flow fixed-bed stainless steel reactor. One gram of the catalyst (40−60 mesh) was packed in the reactor and pretreated in $N_2$ at 400 °C for 2 h. After the catalyst sample was cooled to 200 °C, the sample was purged with 1.3% pyridine−98.7% $N_2$ mixture (30 mL/min) for 1 h and then flushed with $N_2$ for another 1 h. Finally, a reactant gas mixture (5% DME, 35% CO, and 60% $H_2$) was introduced into the reactor at a gas hourly space velocity (GHSV) of 1500 mL/g/h. The reaction pressure was 2.0 MPa. The outlet gas was analyzed online by a gas chromatograph (Agilent 7890A) equipped with TCD and FID detectors using TDX-1 packed column and Pora PLOT Q capillary column, respectively.


DOI: 10.1021/acsami.8b11823
ACS Appl. Mater. Interfaces 2018, 10, 32239−32246

**Scheme 1. Schematic Synthetic Procedure for Spherical Mordenite Zeolite**

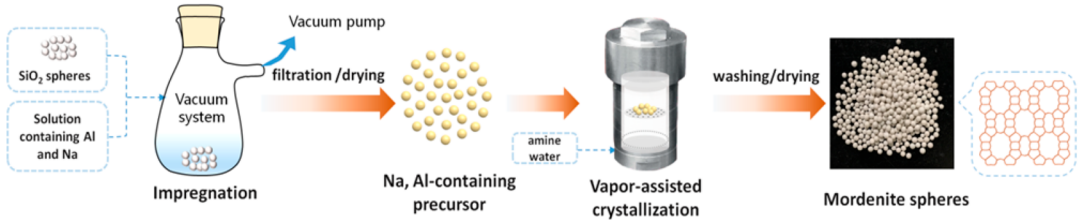


## 3. RESULTS AND DISCUSSION

**3.1. Synthesis and Characterization of Spherical MOR Zeolite Assemblies.** The transformation of porous $SiO_2$ spheres into MOR zeolite was achieved by a vapor-assisted method. The detailed synthetic procedure is shown in Scheme 1. Figure 1a gives the XRD pattern of the spherical silica precursor, which shows a broad halo centered around 22° ($2\theta$) and demonstrates the amorphous nature of the silica precursor. The photograph and SEM images of the silica spheres are displayed in Figure 1b, from which regular spheres with solid interior in sizes of 2−3 mm can be observed. The corresponding $N_2$ adsorption isotherm of the silica precursor is shown in Figure 2a, from which a typical type-IV isotherm could be observed, suggesting the existence of the mesoporous structure. DFT porosity distribution curve (Figure 2b) reveals that the dominant mesopore diameter is centered around 13 nm.

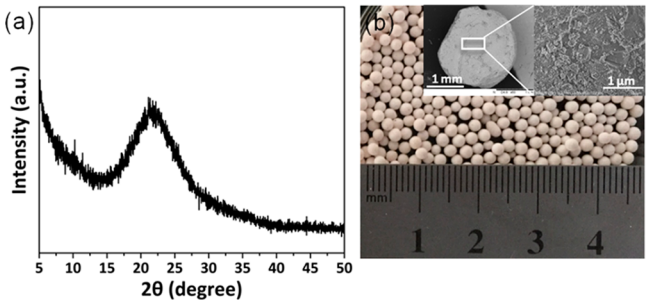


**Figure 1.** (a) XRD pattern and (b) photograph of silica spheres. The inserts in (b) are the SEM images of the cross section of silica sphere at different magnifications.

Spherical MOR zeolite assemblies were synthesized using porous Na- and Al-doped silica spheres as the precursor under the TEAOH vapor at 175 °C for 72 h (denoted as MOR-TEAOH). Figure 3a shows the XRD pattern of sample MOR-TEAOH. No impurity phase was discerned, and all the peaks could be indexed to the MOR structure. The relative crystallinity of the sample is calculated to be 95% comparing with the reference commercial MOR sample (Table 1), which indicates the successful transformation of silica spheres into crystalline mordenite. From the photograph displayed in Figure 3b, it is evident that the morphological feature of the silica spheres is well retained. The SEM images (Figure 3c) reveal that the interior of the spheres is solid with the appearance of some irregular micrometer-sized void space. Further magnification (Figure 3d) shows that the sphere consists of well-crystallized MOR crystals and only small amounts of amorphous materials. This further confirms the

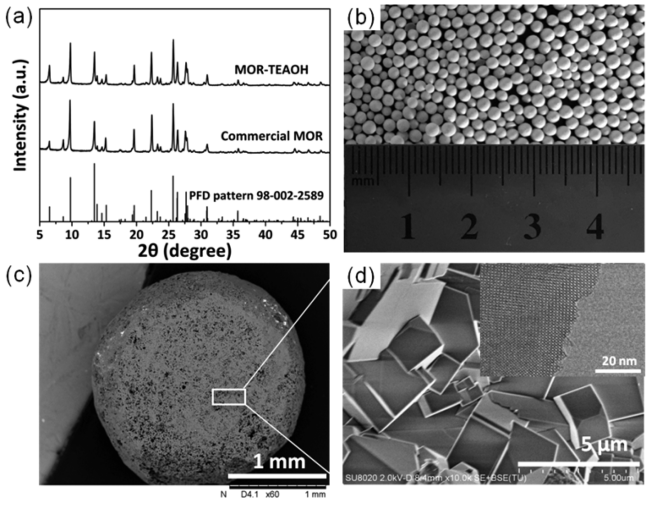


**Figure 3.** (a) XRD patterns of the samples MOR-TEAOH and commercial MOR, (b) photograph of the MOR-TEAOH spheres, (c) SEM image of the cross section of the MOR-TEAOH sphere, (d) SEM image of the MOR crystals in the MOR-TEAOH sphere. The insert in (d) is the TEM image of the MOR crystal in MOR-TEAOH sphere.

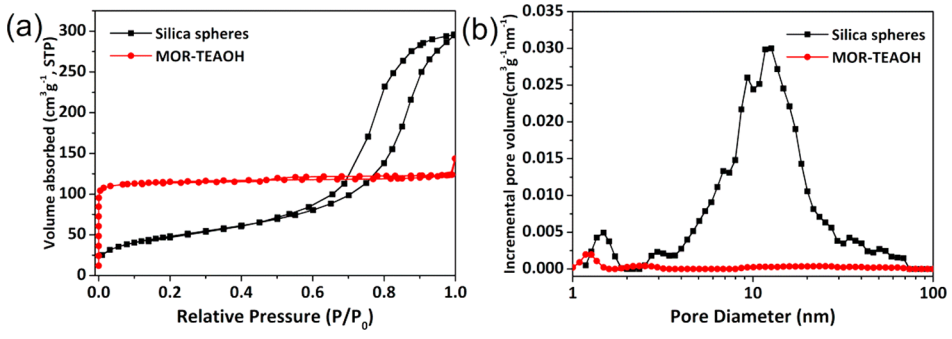


**Figure 2.** (a) $N_2$ adsorption−desorption isotherms and (b) DFT pore size distribution based on adsorption branch of silica spheres and MOR-TEAOH.



DOI: 10.1021/acsami.8b11823
ACS Appl. Mater. Interfaces 2018, 10, 32239−32246

**Table 1. Product Compositions, Textual Properties, and Compressive Strength of the Samples**

| sample | Si/Al[a] | $C_{zeo}$(%)[b] | Si/Al[c] | surface area ($m^2$/g) $S_{BET}$[d] | $S_{micro}$[e] | $S_{ext}$[f] | pore volume ($cm^3$/g) $V_{micro}$[e] | $V_{total}$[g] | relative crystallinity[h] (%) | compressive strength (N) |
|---|---|---|---|---|---|---|---|---|---|---|
| silica spheres | | | | 174 | 2 | 172 | 0 | 0.44 | | 46 |
| MOR-TEAOH | 10.1 | 89.0 | 9.0 | 384 | 340 | 44 | 0.16 | 0.19 | 95 | 38 |
| MOR-TMAOH | 9.4 | 91.3 | 8.6 | 392 | 349 | 42 | 0.16 | 0.20 | 147 | 24 |
| MOR-HMI | 10.0 | 82.3 | 8.2 | 330 | 314 | 15 | 0.15 | 0.15 | 102 | 27 |
| MOR-$H_2O$ | 8.8 | 66.0 | 5.8 | 286 | 252 | 34 | 0.12 | 0.15 | 68 | 29 |
| commercial MOR | 6.5 | | | 418 | 382 | 36 | 0.19 | 0.21 | 100 | |

[a]The Si/Al ratio of the spherical samples detected by XRF. [b]Zeolite content estimated by comparing the micropore areas of the synthesized samples with that of commercial MOR. [c]Zeolite Si/Al ratio estimated according to the product composition and the zeolite content because all the Al atoms were incorporated into the zeolite according to the $^{27}$Al MAS NMR spectra shown in Figure 4 and Figure S1. [d]BET surface area. [e]Calculated by t-plot method. [f]$S_{ext} = S_{BET} - S_{micro}$. [g]Determined from adsorbed volume at $P/P_0 = 0.98$. [h]Calculated from the eight strongest peaks of the samples with commercial MOR as a standard.

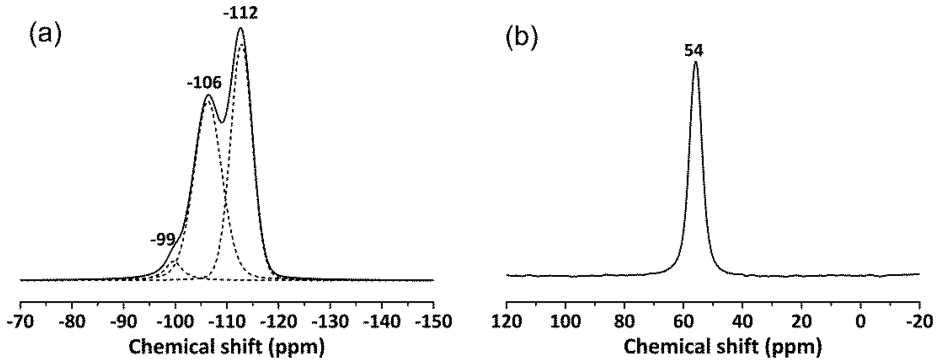


**Figure 4.** $^{29}$Si (a) and $^{27}$Al MAS NMR (b) spectra of the as-synthesized sample MOR-TEAOH.

high conversion of the precursor, consistent with the XRD results. High resolution TEM inspection (insert in Figure 3d) also evidences the good crystallinity of MOR zeolite in the spheres. The average compressive strength of MOR-TEAOH spheres is measured to be 38 N (Table 1). The good mechanical strength should result from the intergrowth of MOR crystals in the spheres.

The $N_2$ adsorption isotherm of MOR-TEAOH is shown in Figure 2a, which presents a type-I isotherm with inconspicuous hysteresis loop in the $P/P_0$ range of 0.45−0.9. The corresponding DFT pore size distribution (Figure 2b) shows that the mesopores observed in the silica spheres disappear in the product, which is in agreement with the conversion of the silica precursor. The textural properties of sample MOR-TEAOH are summarized in Table 1. The micropore surface area and micropore volume are 340 $m^2$/g and 0.16 $cm^3$/g, respectively. By comparing the micropore area of MOR-TEAOH with that of the commercial MOR, the zeolite content in the product is roughly calculated to be about 89% (Table 1). In addition, according to the XRF results (Table 1), the Si/Al ratio of sample MOR-TEAOH is measured to be around 10, a value close to that of the pretreated precursor.

Solid-state $^{29}$Si and $^{27}$Al MAS NMR spectra are recorded to investigate the local atomic environments in the MOR-TEAOH. The $^{29}$Si spectrum shown in Figure 4a exhibits two strong peaks at −112 and −106 ppm and one weak peak at −99 ppm, which should be attributed to the Si(0Al), Si(1Al), and Si(2Al) species in the MOR framework, respectively. Moreover, as MOR-TEAOH contains small amounts of unconverted amorphous silica, these peaks should also include the contribution of silicon hydroxyl species. The $^{27}$Al spectrum (Figure 4b) gives only one sharp resonance at 54 ppm, which is the characteristic peak of tetra-coordinated Al species. The peak position and shape are consistent with those of pure MOR zeolite,[8] implying that all the Al atoms were likely incorporated into the zeolite framework. Correspondingly, the zeolite Si/Al ratio in the MOR-TEAOH was calculated, and a value of 9.0 was obtained and listed in Table 1.

**3.2. Synthesis of Spherical MOR Zeolite under Pure Water and Other Amine Vapors.** To illustrate the importance of organic amine on the crystallization and preservation of morphological feature, syntheses with pure $H_2O$ as the liquid phase (denoted as MOR-$H_2O$) were carried out. The synthetic procedure was similar to that of MOR-TEAOH. The results are given in Table 1, Figure 5 and Figure 6c. It can be seen that although the spherical morphology was preserved, the zeolite content in MOR-$H_2O$ product is only

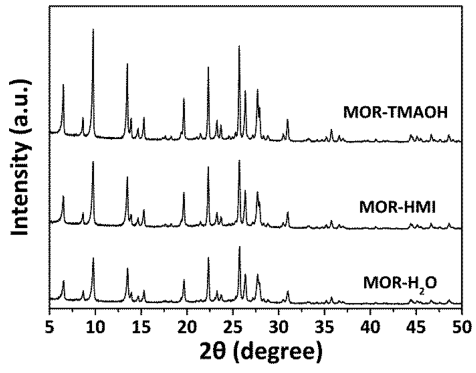


**Figure 5.** XRD patterns of the samples synthesized under pure water and different amine vapors.


DOI: 10.1021/acsami.8b11823
ACS Appl. Mater. Interfaces 2018, 10, 32239−32246

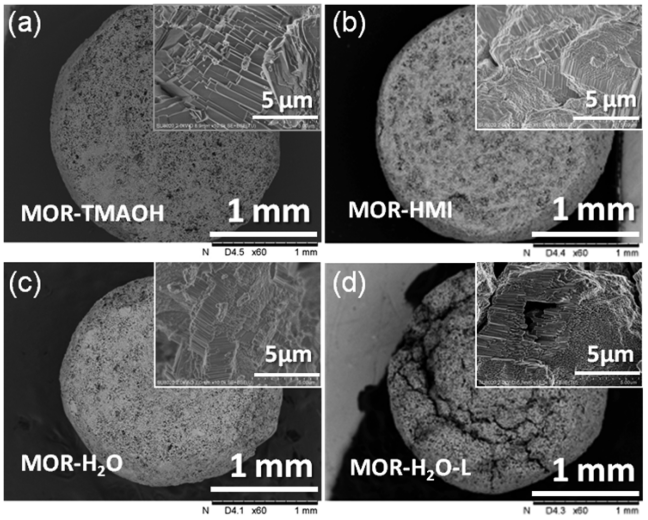


**Figure 6.** SEM images of the cross section of MOR spheres synthesized under water and different amine vapors. The inserts are high-magnification SEM images of the MOR crystals in each sample.

66%, which is clearly lower than those of sample MOR-TEAOH. In an attempt to enhance the zeolite content in MOR-$H_2O$, we found that precursor with higher $OH^-$/Si ratio and lower Si/Al ratio (about 7) is beneficial for the crystallization and a product with zeolite content of 73% can be obtained (denoted as MOR-$H_2O$-L, Table S1). However, cracks appear on the surface of some MOR-$H_2O$-L spheres. And a core−shell structure is formed in the interior of the spherical product, which causes an easy exfoliation of the outer shell (Figure 6d). On the other hand, it is noted that the impregnation treatment under vacuum and the following drying process at ambient temperature are crucial to the successful preparation of the precursors. Otherwise, precursors prepared by impregnation under atmosphere would result in a product with surface cracks or hollow cores (Figure S2). This phenomenon is possibly related to the homogeneity of elemental distribution in the prepared precursors.

It is interesting to note that the present procedure is not limited to TEAOH amine. Tetramethyl hydroxide (TMAOH) and hexamethylenimine (HMI) are also effective for the synthesis (Table 1 and Figures 5, 6, and S3). As can be seen, the samples synthesized could preserve well the spherical morphology, although the MOR crystal morphology varies with the choice of organic amines. The zeolite content for MOR-TMAOH and MOR-HMI is 91.3 and 82.3%, respectively. Obviously, the spherical products synthesized in the presence of TEAOH, HMI, and TMAOH possess zeolite content higher than that of the sample MOR-$H_2O$. The $^{27}$Al MAS NMR spectra of the spherical samples are shown in Figure S1. All the samples give similar spectra with one sharp and strong resonance at 54 ppm, which is similar to that of pure MOR zeolite[8] and suggests that the Al atoms may exist in the zeolite framework. Therefore, the zeolite Si/Al ratio of the products is calculated and shown in Table 1. Higher zeolite Si/Al ratios are found for the products synthesized under the assistance of organic amines. These results demonstrate that the presence of organic amine vapors could promote the crystallization of the spheres and help improve the Si/Al ratio of MOR crystals. Given that the framework stability of medium/low Si zeolites rises with the increase of Si/Al ratio, herein the higher zeolite Si/Al ratio of MOR-amine, as compared with that of MOR-$H_2O$, is expected to be favorable for the catalytic application.

Previous works have shown that TEAOH and HMI are effective organic templates for the synthesis of MOR,[24,25] while TMAOH has not been reported yet. Herein, thermal analyses were conducted to investigate the incorporation of the amines. As shown in Figure S4, all samples synthesized under the assistance of organic amines present weight losses at higher temperatures accompanied by exothermic peaks, evidencing the involvement of organic amines in the crystallization. The content of amines in the products is in the order of HMI > TEAOH > TMAOH. The thermal analysis results are also consistent with the lower Na/Al ratios of the as-synthesized MOR (amine) spheres (Table S2), confirming the partial charge-compensating role of the amines in the crystals.

**3.3. Distribution of $H^+$ Sites in Spherical MOR-TEAOH and Commercial MOR.** Given that the carbonylation performance of the samples is closely related to their Brønsted acidity,[26] the distribution and capacity of the Brønsted acid sites were investigated by $^1$H MAS NMR spectra. Commercial

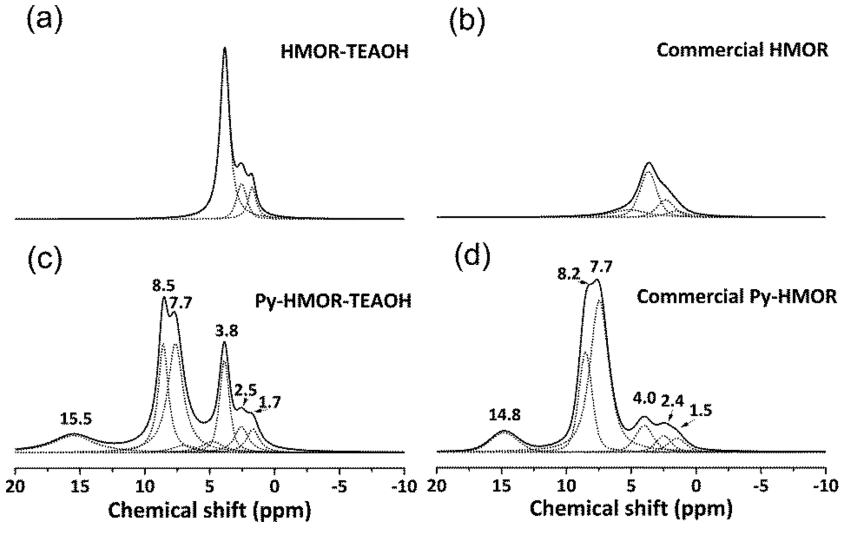


**Figure 7.** $^1$H MAS NMR spectra of the samples before (a and b) and after (c and d) adsorbing pyridine.


DOI: 10.1021/acsami.8b11823
ACS Appl. Mater. Interfaces 2018, 10, 32239−32246

MOR synthesized under inorganic system (Table 1 and Figure S5) herein was used as a reference sample, which has similar total acid amounts to MOR-TEAOH as evidenced by $NH_3$-TPD (Figure S6).

Because pyridine could be absorbed only in the 12-MR channels, a comparison of the spectra measured on the original MOR spheres and the pyridine-adsorbed sample could help us draw a distribution map of the Brønsted acid sites (Figure 7). The corresponding deconvolution results are listed in Table 2.

**Table 2. Acid Capacity of the Samples Calculated Based on the $^1$H MAS NMR Spectra and $NH_3$-TPD**

| | Brønsted acid amount from $^1$H MAS NMR (mmol/g) | | | |
|---|---|---|---|---|
| sample | total | 8-MR | 12-MR | acid amount from $NH_3$-TPD (mmol/g) |
| MOR-TEAOH | 1.02 | 0.76 | 0.26 | 1.61 |
| commercial MOR | 0.78 | 0.39 | 0.39 | 1.73 |

It can be found that the general quantity of Brønsted acid sites in sample MOR-TEAOH is higher than in commercial MOR. Besides, for sample MOR-TEAOH, the amount of Brønsted acid sites in the 8-MR side pockets is calculated to be three times higher than that in 12-MR. This ratio is higher than that of the commercial MOR and most MOR zeolites reported in the literature,[3,27,28] indicating that the present synthetic strategy facilitates the preferential locating of Al atoms (acid sites) in the 8-MR of MOR zeolite. Likely, both the use of TEAOH and the present resources status exert influence on the Al distribution. Moreover, it is noted that the overall acid sites of the two catalysts calculated from both $^1$H MAS NMR and $NH_3$-TPD are inconsistent with their Si/Al ratios (Table 1). It is speculated that dealumination and/or dehydroxylation occur during the calcination process for commercial sample (having lower Si/Al ratio) and cause its lower Brønsted acid concentration.[29]

**3.4. Catalytic Performance in DME Carbonylation.** The DME carbonylation performance of the protonated MOR-TEAOH was investigated on a high-pressure fixed-bed microreactor. Commercial MOR sample was employed as a reference sample. Herein, pyridine-adsorbed catalysts were used for the catalytic evaluation because previous works have shown that the Brønsted acid sites in 8-MR side pockets of MOR zeolite are the unique active sites for the reaction,[3,4] and pyridine adsorption (kinetic diameter 0.58 nm) could selectively poison the acid sites in the 12-MR channel and help avoid the side reactions of reactant and product when diffusing through the main channels.

The DME conversion and MAc selectivity versus time on stream over the samples are shown in Figure 8. At the very beginning of the reaction, both samples exhibited a low DME conversion, corresponding to the induction period, in which DME molecules interacted with Brønsted acid sites to form surface methoxyl species, which act as the true active centers in the DME carbonylation reaction.[26] As the reaction went on, the DME conversion on MOR-TEAOH increased rapidly and achieved a relatively steady value of ~90% after 4 h on stream. The steady conversion on commercial MOR sample was, however, only about 23%. In combination with the above characterization results, the excellent catalytic activity of MOR-TEAOH should come from the large amount of Brønsted acid sites in the 8-MR side pockets. Moreover, although both samples gave high selectivity to the desired product MAc, a slightly better selectivity could be discerned over the MOR-TEAOH catalyst. This might be related to the lower acid density in the 12-MR channels of MOR-TEAOH (smaller amount of pyridine adsorption), which leaves more free space in the main channels for the diffusion of reactants and products and thus decreases side reactions and leads to a higher MAc selectivity. The MAc synthesis rate per $H^+$ sites in the 8-MR side pockets of the catalysts was calculated and listed in Table S3, which gives 3.60 mol/($mol_{acid}$ h) for MOR-TEAOH and 1.75 mol/($mol_{acid}$ h) for commercial MOR. The lower MAc synthesis rate on the commercial MOR likely results from the bad accessibility of the $H^+$ sites in the 8-MR side pockets, which was caused by the dealumination as deduced from the acid characterization results.

## 4. CONCLUSIONS

In summary, an amine-assisted dry-gel transformation method was developed to prepare millimeter-sized spherical MOR zeolite by using commercial silica spheres as a precursor. The intergrowth of MOR crystallines in the spheres helps the product show good mechanical strength. Three amines, including TEAOH, TMAOH and HMI, were found to be effective for the synthesis of MOR spheres. The appearance of organic amine in the synthesis vapor can help achieve well-retained morphology, promote the crystallization, and improve the Si/Al ratio of MOR crystallines. Abundant $H^+$ sites were revealed to locate in the 8-MR side pockets (0.76 mmol/g) of spherical MOR-TEAOH, which amounted to 75% of the total $H^+$ sites. These values are obviously higher than those of

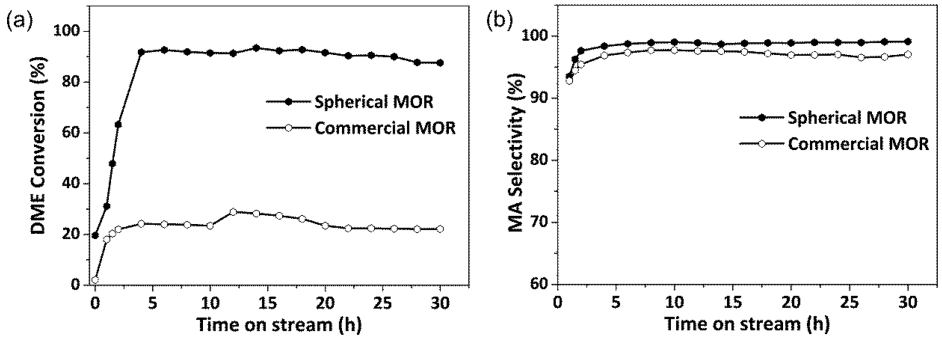


**Figure 8.** DME conversion and MAc selectivity with time on stream on the pyridine-adsorbed samples. Reaction conditions: 200 °C, 2.0 MPa, 1500 mL/g/h, DME/CO/$H_2$ = 5/35/60 (vol).


DOI: 10.1021/acsami.8b11823
ACS Appl. Mater. Interfaces 2018, 10, 32239−32246

reference sample (0.39 mmol/g in the 8-MR, 50%). Due to the preferential siting of $H^+$ sites in the 8-MR side pockets, MOR-TEAOH shows excellent catalytic activity in the DME carbonylation reaction with a steady DME conversion of 90%, whereas only about 23% conversion on the commercial sample.

## ■ ASSOCIATED CONTENT

### Supporting Information

The Supporting Information is available free of charge on the ACS Publications website at DOI: 10.1021/acsami.8b11823.

$^{27}$Al MAS NMR, SEM image, $N_2$ adsorption and desorption isotherm, thermogravimetric analysis, and $NH_3$-TPD (PDF)

## ■ AUTHOR INFORMATION


### Corresponding Authors

*E-mail: tianpeng@dicp.ac.cn.

*E-mail: liuzm@dicp.ac.cn.

### ORCID

Zhongmin Liu: 0000-0001-8439-2336


### Notes

The authors declare no competing financial interest.

## ■ ACKNOWLEDGMENTS

This work was supported by the National Natural Science Foundation of China (Grants 21476228, 21676262, and 21506207) and the Key Research Program of Frontier Sciences, CAS (QYZDB-SSW-JSC040).

## ■ REFERENCES


(1) Cheung, P.; Bhan, A.; Sunley, G. J.; Iglesia, E. Selective Carbonylation of Dimethyl Ether to Methyl Acetate Catalyzed by Acidic Zeolites. *Angew. Chem., Int. Ed.* **2006**, *45* (10), 1617−1620.

(2) Rasmussen, D. B.; Christensen, J. M.; Temel, B.; Studt, F.; Moses, P. G.; Rossmeisl, J.; Riisager, A.; Jensen, A. D. Ketene as a Reaction Intermediate in the Carbonylation of Dimethyl Ether to Methyl Acetate over Mordenite. *Angew. Chem., Int. Ed.* **2015**, *54* (25), 7261−7264.

(3) Bhan, A.; Allian, A. D.; Sunley, G. J.; Law, D. J.; Iglesia, E. Specificity of Sites within Eight-Membered Ring Zeolite Channels for Carbonylation of Methyls to Acetyls. *J. Am. Chem. Soc.* **2007**, *129* (16), 4919−4924.

(4) Boronat, M.; Martinez-Sanchez, C.; Law, D.; Corma, A. Enzyme-Like Specificity in Zeolites: A Unique Site Position in Mordenite for Selective Carbonylation of Methanol and Dimethyl Ether with CO. *J. Am. Chem. Soc.* **2008**, *130* (48), 16316−16323.

(5) San, X.; Zhang, Y.; Shen, W.; Tsubaki, N. New Synthesis Method of Ethanol from Dimethyl Ether with a Synergic Effect Between the Zeolite Catalyst and Metallic Catalyst. *Energy Fuels* **2009**, *23* (5), 2843−2844.

(6) Zhang, Z. H. China Creates World's First Coal-to-Ethanol Production Line. http://www.chinadaily.com.cn/china/2017-03/17/content_28595237.html (accessed March 17, 2017).

(7) Ma, M.; Huang, X. M.; Zhan, E. S.; Zhou, Y.; Xue, H. F.; Shen, W. J. Synthesis of Mordenite Nanosheets with Shortened Channel Lengths and Enhanced Catalytic Activity. *J. Mater. Chem. A* **2017**, *5* (19), 8887−8891.

(8) Yuan, Y. Y.; Wang, L. Y.; Liu, H. C.; Tian, P.; Yang, M.; Xu, S. T.; Liu, Z. M. Facile Preparation of Nanocrystal-Assembled Hierarchical Mordenite Zeolites with Remarkable Catalytic Performance. *Chin. J. Catal.* **2015**, *36* (11), 1910−1919.

(9) Kim, J.; Jo, C.; Lee, S.; Ryoo, R. Bulk Crystal Seeding in the Generation of Mesopores by Organosilane Surfactants in Zeolite Synthesis. *J. Mater. Chem. A* **2014**, *2* (30), 11905−11912.

(10) Tang, T.; Zhang, L.; Fu, W.; Ma, Y.; Xu, J.; Jiang, J.; Fang, G.; Xiao, F.-S. Design and Synthesis of Metal Sulfide Catalysts Supported on Zeolite Nanofiber Bundles with Unprecedented Hydrodesulfurization Activities. *J. Am. Chem. Soc.* **2013**, *135* (31), 11437−11440.

(11) Dědeček, J.; Sobalík, Z.; Wichterlová, B. Siting and Distribution of Framework Aluminium Atoms in Silicon-Rich Zeolites and Impact on Catalysis. *Catal. Rev.: Sci. Eng.* **2012**, *54* (2), 135−223.

(12) Biligetu, T.; Wang, Y.; Nishitoba, T.; Otomo, R.; Park, S.; Mochizuki, H.; Kondo, J. N.; Tatsumi, T.; Yokoi, T. Al Distribution and Catalytic Performance of ZSM-5 zeolites Synthesized with Various Alcohols. *J. Catal.* **2017**, *353*, 1−10.

(13) Pashkova, V.; Sklenak, S.; Klein, P.; Urbanova, M.; Dědeček, J. Location of Framework Al Atoms in the Channels of ZSM-5: Effect of the (Hydrothermal) Synthesis. *Chem. - Eur. J.* **2016**, *22* (12), 3937−3941.

(14) Roman-Leshkov, Y.; Moliner, M.; Davis, M. E. Impact of Controlling the Site Distribution of Al Atoms on Catalytic Properties in Ferrierite-Type Zeolites. *J. Phys. Chem. C* **2011**, *115* (4), 1096−1102.

(15) Park, S. Y.; Shin, C.-H.; Bae, J. W. Selective Carbonylation of Dimethyl Ether to Methyl Acetate on Ferrierite. *Catal. Commun.* **2016**, *75*, 28−31.

(16) Li, X.; Chen, X.; Yang, Z.; Zhu, X.; Xu, S.; Xie, S.; Liu, S.; Liu, X.; Xu, L. Seed-Assisted Synthesis of FER/MOR Composite Zeolite and its Specific Catalytic Application in Carbonylation Reaction. *Microporous Mesoporous Mater.* **2018**, *257*, 79−84.

(17) Melero, J. A.; Calleja, G.; Martinez, F.; Molina, R.; Pariente, M. I. Nanocomposite $Fe_2O_3$/SBA-15: An Efficient and Stable Catalyst for the Catalytic Wet Peroxidation of Phenolic Aqueous Solutions. *Chem. Eng. J.* **2007**, *131* (1−3), 245−256.

(18) Ali, M. A.; Tatsumi, T.; Masuda, T. Development of Heavy Oil Hydrocracking Catalysts Using Amorphous Silica-Alumina and Zeolites as Catalyst Supports. *Appl. Catal., A* **2002**, *233* (1−2), 77−90.

(19) Tsai, R. F.; Du, K. J.; Cheng, T. Y.; Ho, G. H.; Wu, P. H.; Liu, S. B.; Tsai, T. C. Solid-State Synthesis of Mesoporous MFI Zeolite from Self-Bonded Silica Pellets. *Catal. Today* **2013**, *204*, 30−37.

(20) Wang, H. T.; Huang, L. M.; Wang, Z. B.; Mitra, A.; Yan, Y. S. Hierarchical Zeolite Structures with Designed Shape by Gel-Casting of Colloidal Nanocrystal Suspensions. *Chem. Commun.* **2001**, No. 15, 1364−1365.

(21) Peppel, T.; Paul, B.; Kraehnert, R.; Enke, D.; Lucke, B.; Wohlrab, S. Shape-Preserving Transformation of Monolithic Porous Glass into MFI-Type Zeolite. *Microporous Mesoporous Mater.* **2012**, *158*, 180−186.

(22) Wang, D. J.; Liu, Z. N.; Xie, Z. K. Preparation of Binder-Free Utrafine ZSM-5 Zeolite Monoliths by Vapor-Phase Transformation Method. *Wuji Cailiao Xuebao* **2008**, *23* (3), 592−596.

(23) Mintova, S.; Hölzl, M.; Valtchev, V.; Mihailova, B.; Bouizi, Y.; Bein, T. Closely Packed Zeolite Nanocrystals Obtained via Transformation of Porous Amorphous Silica. *Chem. Mater.* **2004**, *16* (25), 5452−5459.

(24) Lu, B. W.; Oumi, Y.; Itabashi, K.; Sano, T. Effect of Ammonium Salts on Hydrothermal Synthesis of High-Silica Mordenite. *Microporous Mesoporous Mater.* **2005**, *81* (1−3), 365−374.

(25) Lv, A. L.; Xu, H.; Wu, H. H.; Liu, Y. M.; Wu, P. Hydrothermal Synthesis of High-Silica Mordenite by Dual-Templating Method. *Microporous Mesoporous Mater.* **2011**, *145* (1−3), 80−86.

(26) Cheung, P.; Bhan, A.; Sunley, G. J.; Law, D. J.; Iglesia, E. Site Requirements and Elementary Steps in Dimethyl Ether Carbonylation Catalyzed by Acidic Zeolites. *J. Catal.* **2007**, *245* (1), 110−123.

(27) Li, B. J.; Xu, J.; Han, B.; Wang, X. M.; Qi, G. D.; Zhang, Z. F.; Wang, C.; Deng, F. Insight into Dimethyl Ether Carbonylation Reaction over Mordenite Zeolite from In-Situ Solid-State NMR Spectroscopy. *J. Phys. Chem. C* **2013**, *117* (11), 5840−5847.

(28) Zhou, H.; Zhu, W. L.; Shi, L.; Liu, H. C.; Liu, S. P.; Ni, Y. M.; Liu, Y.; He, Y. L.; Xu, S. L.; Li, L. N.; Liu, Z. M. In Situ DRIFT Study of Dimethyl Ether Carbonylation to Methyl Acetate on H-Mordenite. *J. Mol. Catal. A: Chem.* **2016**, *417*, 1−9.
(29) Miller, J. T.; Hopkins, P. D.; Meyers, B. L.; Ray, G. J.; Roginski, R. T.; Zajac, G. W.; Rosenbaum, N. H. The Effect of Nonframework Aluminum on Acidity in Dealuminated Mordenite. *J. Catal.* **1992**, *138* (1), 115−128.


DOI: 10.1021/acsami.8b11823
*ACS Appl. Mater. Interfaces* 2018, 10, 32239−32246